IEEE Access
Multidisciplinary | Rapid Review | Open Access Journal

Received December 8, 2020, accepted December 21, 2020, date of publication December 24, 2020, date of current version January 6, 2021.

*Digital Object Identifier 10.1109/ACCESS.2020.3047103*

# Investigation of 2D Nano-Structured Winding Insulation for High Torque Density Medium-Voltage Motor

**HIEP HOANG NGUYEN[1], (Member, IEEE), ARSHIAH Y. MIRZA[1], (Graduate Student Member, IEEE), WEIQIANG CHEN[1], (Member, IEEE), YIQI LIU[1], JOANNE RONZELLO[2], JACK CHAPMAN[3], ALI M. BAZZI[1], (Senior Member, IEEE), AND YANG CAO[1,2], (Senior Member, IEEE)**

[1]Department of Electrical and Computer Engineering, University of Connecticut, Storrs, CT 06269, USA
[2]Electrical Insulation Research Center, Institute of Materials Science, University of Connecticut, Storrs, CT 06269, USA
[3]General Dynamic Electric Boat, Groton, CT 06340, USA

Corresponding author: Yang Cao (yang.cao@uconn.edu)

This work was supported by the U.S. Office of Naval Research under Grant N00014-15-1-2413 and Grant N00014-19-1-2306.

**ABSTRACT** Since the introduction of mica paper and synthetic resin-based taping insulation for rotating-machines in 1950s, only evolutional improvements in their properties and processing have been made. Due to its challenging nature, much of recent insulation research has been focused on the aspect of reliability rather than performance enhancement. This paper presents the development and performance evaluation of a revolutionary nanostructured insulation in the manufacturing of large propulsion motors with game-changing torque density and payload efficiency for marine Next Generation Integrated Power System. It is demonstrated that nanostructured insulation based on 2D-platelet fillers could offer significant improvement over conventional insulation system in electrical, dielectric, thermal and mechanical properties. Optimal nanostructured insulation formation identified through a Design of Experiment study exhibits high thermal conductivity of $>0.8$ W/(m·K), high breakdown strength of $>40$ kV/mm, low dielectric constant of less than 5.5 and low dielectric loss factor of less than 2.5% at 155°C. Voltage endurance tests on coupons with optimal formulation, in accordance with IEC 60343 standard, demonstrate satisfactory endurance life. Furthermore, a multi-physics finite-element-analysis model of the winding in a medium-voltage electric motor is established to perform electromagnetic and thermal analyses in ANSYS under various temperature boundary conditions. The study indicates a remarkable increase of 14% in torque handling capacity of a motor wound with proposed nanostructured insulation material when compared to an identical motor wound with conventional micaceous insulation.

**INDEX TERMS** Nanostructured insulation, voltage endurance, discharge resistance, multi-physics simulation, medium-voltage induction machines, propulsion motor, stator insulation.

## I. INTRODUCTION

As U.S Navy embraces All Electric Ship (AES) platform where electrical power for both propulsion and service loads is provided through the integrated power system (IPS), there are rapidly growing demands for power/torque density and payload efficiency for marine propulsion and power generation [1]. While AC synchronous high temperature superconductor (HTS) motors and permanent magnet motors could offer high power dense propulsion, the Navy is interested in improving payload efficiency of advanced induction motors (AIMs), due to their high scalability, affordability, large industrial base, and full dynamic range of high efficiency operation [1]–[5].

Existing high power/torque motors require either direct- or indirect- liquid cooling with extra cooling/cryogenic systems [6]–[12]. For direct water cooling, cooling path through stator coils at Medium Voltage (MV) is challenging and requires special de-ionized water cooling systems to reduce conduction losses through the coolant from phase-phase and

The associate editor coordinating the review of this manuscript and approving it for publication was Pinjia Zhang.

phase-ground and also to reduce corrosion of the copper conductors. For indirect cooling tubes embedded in the stator coils, the same level of MV insulation is required between the conductors and the cooling tubes at ground potential. Embedded tubing or through conductor cooling passage also takes away from the limited space in the slot for copper conductors, causing further increases in stator resistance, ohmic losses, and heat generation. Furthermore, the hot spots in end turns require additional conduction path or cooling loops. Hence, it will be highly desirable to develop a water-free heat dissipation solution for propulsion motor with high torque density and efficiency.

This could be achieved through forced air cooling of AIM machine to largely reduce the thermal resistance across winding insulation. At present, MV propulsion motors rely on micaceous tape insulation manufactured with vacuum-pressure-impregnation (VPI) process [15]. The greatest concentration of heat inside a propulsion motor occurs in the copper strands of the winding. The primary path for heat removal starts from the copper conductor heat source, conducts through a series of successive thermal resistances in the ground-wall insulation (conductor shield, mica tape insulation), armature, corona shield, side springs, slot liners, iron, and finally to the stator cooling ducts. The largest temperature gradient identified corresponds to the temperature differential across the insulation, indicating the dominant role that the thermal resistance of stator insulation plays in the temperature of stator copper in MV motors.

State-of-the-art ground-wall insulation is based predominantly on micaceous with multiple layers of taped glass-fabric reinforced mica paper, bonded together with epoxy binder. Mica is a group of phyllosilicate minerals (muscovite) with a layered platelet crystalline structures that can be split or delaminated into thin sheets texture to offer superior electrical discharge resistance [16], [17]. However, the flaky structures of muscovite mica correspond to a very low through-plane thermal conduction. Its limited elongation capability leads also to crack and voids formation under rapid thermal loads and constant double frequency magnetic force [18]. The delamination and voids will not only further reduce heat conduction, but also support electrical partial discharge that leads to the aging and failure of machine. In addition, resin pockets between plys of tapes and non-impregnated voids within mica paper lead to overall limited electrical, thermal, and mechanical performance for micaceous insulation system.

A nanostructured winding insulation has been developed to offset the performance limit of existing micaceous insulation (Section II). Figure 1 illustrates the strategy to transform the basic research of proposed nanostructured insulation material to electric propulsion motor with game changing torque density, manufacturable by new (additive) processes [13]. The nanostructured insulation material was constructed using 2D nanoplatelets of nanoclays (talc-pyrophyllite magnesium silicate) and stacked layers of nitride nanoplatelets, with each layer thickness being on the order of 1 nm, uniformly

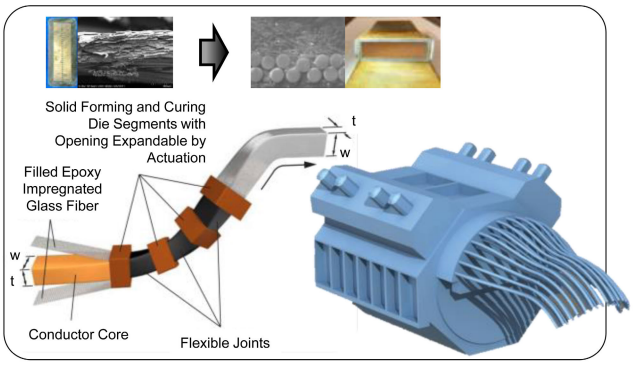


**FIGURE 1. Nanostructured winding insulation for electric propulsion motor with gaming changing torque density. Schematics for additive manufacturing and AIM motor are taken from Refs. 13-14.**

dispersed in epoxies with preferred orientation to achieve desirable characteristics of electrical discharge resistance and high thermal conduction [19], [20]. Section III gives a brief description of the thermal and electromagnetic simulations and evaluates the electromagnetic and thermal performance of MV motors with nanostructured insulation material (NIM) vs micaceous insulation material (MIM). Section IV concludes the paper.

## II. NANOSTRUCTURED INSULATION CHARACTERISTICS

To identify optimal nanostructured insulation formulation, a mixture Design of Experiment (DoE) was implemented, using software Minitab to systematically investigate the relationships between input variables and output responses, with nearly 100 formulation runs, benchmarking against the performance metrics of micaceous insulation. The design inputs include the percentile filler concentrations and processing conditions. The output responses correspond to major performance metrics, including thermal conductivity, ac breakdown strength, complex dielectric permittivity, which were characterized using thermal conductivity meter TA DTC-300, dielectric breakdown tester BAUR DTA-100C, Agilent 4284 Precision LCR meter, respectively. The nanostructured material samples of each formulation were fabricated and tested accordingly. The testing result data were then fed into the DoE analysis which statistically predicts the output responses. A set of targeted performance metrics responses was established as following: the thermal conductivity of 0.8- 0.9 W/(m·K), ac breakdown strength of 40- 44 kV/mm (1000- 1100 VPM, with VPM stands for volt per mil), dissipation factor of 0.2- 0.3, and dielectric constant of 4- 5. The DoE analysis estimated a range of filler concentrations, indicated between the solid and the dash lines of contour plot, for each targeted response, as shown in Figure 2. In particular, the dissipation factor was $<0.3$ for the entire design space of variables. By overlaying the contour plots of multiple targeted responses, an optimal region of design for nanostructured insulation formulations, which simultaneously satisfied all targeted performance metrics, was identified as highlighted in Figure 2.

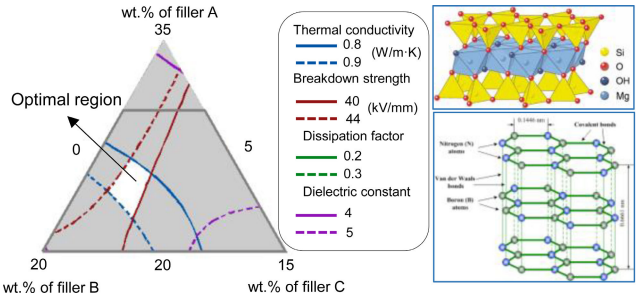


**FIGURE 2.** Overlaid contour plots for mixture DoE with highlighted optimal design region, satisfying simultaneously the thermal, electrical, and dielectric requirements. All the fillers investigated possess 2D layered structures.

**TABLE 1.** MV motor insulation system performance metrics.

| | Micaceous | Nano ExhibA | Nano ExhibB |
|---|---|---|---|
| **Thermal Class** | F, H | F, H | F, H |
| **Operating Strength** | 2.6 kV/mm (~65VPM ) | 4 kV/mm (100VPM ) | 4 kV/mm (100VPM ) |
| **Thermal Conductivity** | 0.25 W/(m·K) | 1.0 W/(m·K) | 0.9 W/(m·K) |
| **Dielectric Strength** | 30 kV/mm (750 VPM) | 47 kV/mm (1175 VPM) | 43 kV/mm (1075 VPM) |
| **Loss Factor** | >3% | <2.5% | <2.5% |
| **Strain** | <0.3% | >1% | >1% |
| **Manufacturing** | Taping/VPI | Additive | |

Based on the outcome of DoE, exemplar nanostructured formulations of Nano ExhibA and Nano ExhibB were selected and fully characterized. The performance characteristics of these materials are shown in Figure 3 and summarized in Table 1, benchmarking against MIM. Except for ac breakdown strength, all the characterizations were conducted as a function of temperature from room temperature to class F (155°C). Both nanostructured insulation formulations obtain superior properties over the MIM. As seen in Figure 3(a), NIMs show much lower dielectric constants with nearly no dispersion in the frequency and temperature ranges studied, which is preferred due to lower stress concentration in defects like air pockets so that partial discharge is less likely to take place. Their corresponding dielectric loss factor at 155°C is also much lower than micaceous insulation. While the dielectric loss factor for micaceous insulation reaches 5% at 155°C, the loss factors for both Nano ExhibA and B are as low as 2.5%, shown in Figure 3(b). More importantly, Figure 3(c) indicates that NIMs exhibit largely enhanced thermal conductivity of >0.9 W/(m·K) over that of micaceous at only ∼ 0.25 W/(m·K). The dielectric breakdown strength of NIMs records also large improvement over micaceous insulation (MIM) by ∼30% as shown in Figure 3(d).

Furthermore, for MV/HV electric machines, partial discharge is inevitable which aggressively attacks the insulation material, leading to premature failure of the machines. Therefore, the voltage endurance test was performed in accordance with IEC- 60343 standard to evaluate the discharge resistance of new insulation materials, as shown in Figure 4. Disk coupons with diameter of 10 cm of Nano ExhibA and Nano ExhibB were fabricated and subjected to the voltage endurance test, along with neat epoxy baseline. The sample configuration and experimental setup are shown in Figure 4. With the application of high voltage, electrical discharge was generated around the high voltage electrode. The corona discharge tends to spread out on the surface of the samples and attempts to develop into streamers that flashover along the sample surface to the ground electrode. For each sample composition, at least five replicas were fabricated for testing.

As shown in Figure 4, this discharge resistance test represents one of the most stringent HV tests with intense electrical discharges developed on the sample surface. Under the bombardment and erosion of electrical discharges (plasma), the surface of the samples will gradually be eroded away due to the loss of materials. In order to quantitatively study the geometrical degradation of the surface erosion under discharge, 3D profilometry was obtained by using a Keyence VHX-2000 Digital Microscope, as shown in Figure 5 the topology profiles. The 3D-profilometry of the surface erosion for samples subjected to 270 h of testing are shown in the left (Figure 5 a, b, c), with the circle in the center of each photo represents the position of the high voltage electrode. Visual inspection suggests there is a huge difference between epoxy resin sample and the nanostructured insulation samples regarding their degrees of degradation. As can be further seen quantitatively in the corresponding topology profiles in Figure 5(a), the neat epoxy sample exhibited fully developed erosion channels, distributed radially out from the edge of high voltage electrode, with the erosion depth that can reach as much as 0.6 mm. On the other hand, nanocomposite samples showed varying but minor degrees of erosion. The surfaces of Nano ExhibA and Nano ExhibB samples were still fairly smooth and flat with a maximum erosion depth of only <60 $\mu$m (Figure 5 b, c). With the extension of the discharge aging, the surface erosion progressed substantially for the neat epoxy. On the surface of the neat epoxy −568 h (Figure 5 d), the erosion channels became much deeper and wider, with the depth reaching >1 mm, which caused puncture-through breakdown of the sample. The site of breakdown was the small, darkened spot close to the edge of high voltage electrodes, indicated by a black arrow in Figure 5(d). In striking contrast, the surfaces of Nano ExhibA- 1086 h and Nano ExhibB- 1720 h were still flat, marked with only minor erosion and the maximum erosion depth was <200 $\mu$m (Figure 5 e, f).

The key characteristic of voltage endurance tests is the *time to failure*. As shown in Figure 6, both Nano ExhibA and Nano ExhibB samples recorded satisfactory endurance lifetime of >2500 h (according to IEEE 1043/1553 standards, an endurance life of 400 h usually corresponds to an equivalent 30 years of service life).

In summary, the new nanostructured winding insulation offers a combined improvement of

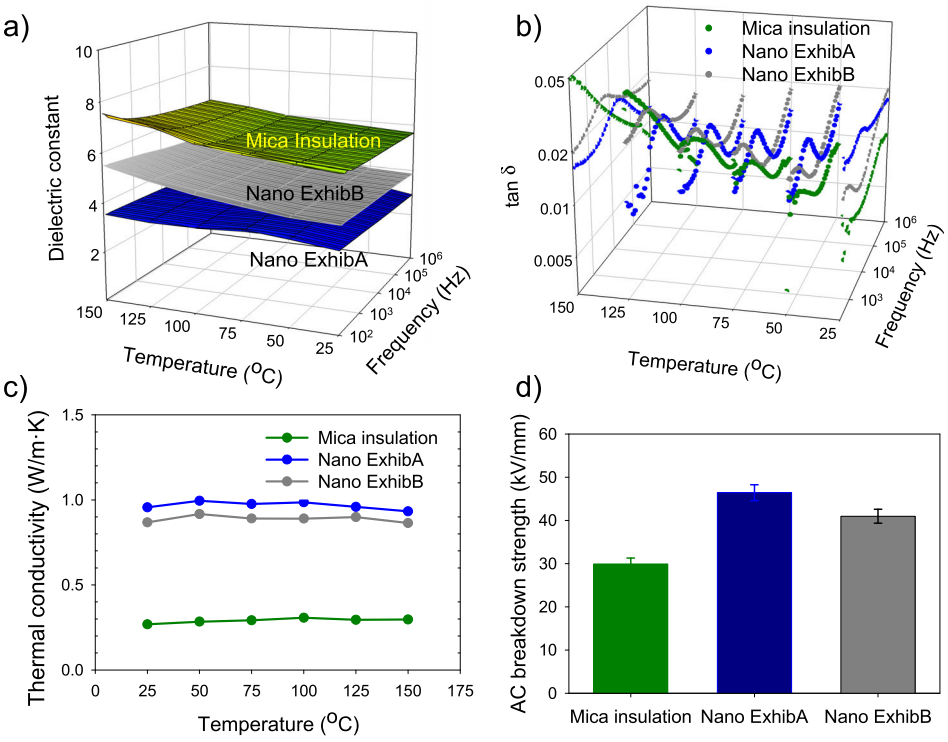


**FIGURE 3.** Properties of nanostructured insulation materials Nano ExhibA and Nano ExhibB, benchmarking against micaceous insulation for (a) dielectric constant, (b) dielectric loss factor (tan $\delta$), (c) thermal conductivity, and (d) ac breakdown strength. Except for ac breakdown strength, all the characterizations were conducted as a function of temperature from room temperature to class F (155°C).

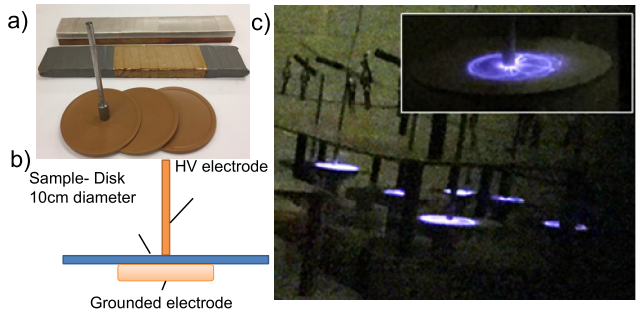


**FIGURE 4.** Test setup for voltage endurance test according to IEC- 60343. a) Examples of nanostructured disk coupons and model stator bars, b) Electrodes-sample configuration, c) Experimental setup under the test. Inset shows intense electrical discharges on a sample surface under high voltage stress.

- high dielectric strength of > 40 kV/mm (1000 VPM) and excellent voltage endurance life, with the promise of an enhanced operating strength of 4 kV/mm (100 VPM), which translates to
- reduced insulation wall thickness for higher copper filling ratio and reduced copper loss
- additional >2X improved thermal conductivity in ground-wall insulation
- crack resistance insulation enabling a new integrated armature/corona-shield structure with lower thermal resistance

More importantly, the new nanostructured insulation opens the door for new manufacturing processes of the winding insulation, such as the additive manufacturing [13]. As shown schematically in Figure 1, a new manufacturing process will reduce the bar shape variation, whereas non-uniform insulation thickness often occurs in the conventional taping/VPI process of micaceous insulation. Hence, the side clearance between the stator bars and slots, and the associated thermal resistance can be significantly reduced. This paradigm shift holds the promise to revolutionize electrical insulation in the manufacturing of propulsion motor with game-changing torque density and payload efficiency, as will be demonstrated next in machine modeling studies.

## III. THERMAL AND ELECTROMAGNETIC STUDY

### A. GEOMETRY - RMxprt

The electromagnetic and thermal analyses were performed using ANSYS Maxwell. A customized MV induction machine was simulated based on NIM and MIM. The machine design was conducted using the RMxprt tool in ANSYS Maxwell, which is a template-based tool for fast design of electric machines. All the physical measurements, geometry, machine parameters, and other specifications of the machine are summarized in Table 2 . The operating fields of the ground-wall insulation were set at 2.6 kV/mm (65 VPM) for both computational study cases, while the

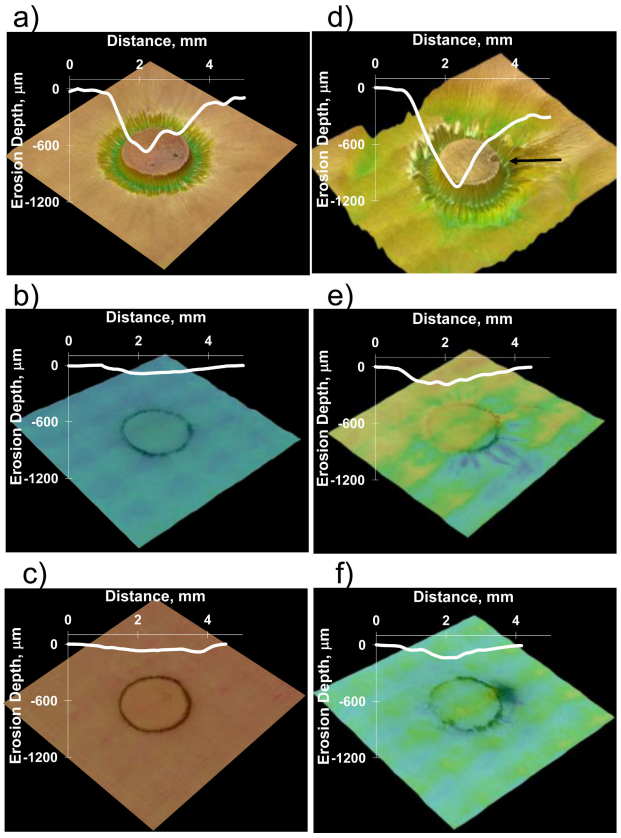


**FIGURE 5.** 3D - Profilometry of 2.5 mm thick samples after voltage endurance aging under 10 kV/mm (250 VPM). a) neat epoxy- 270 h; b) Nano ExhibA- 270 h; c) Nano ExhibB- 270 h; d) neat epoxy – 568 h; e) Nano ExhibA -1086 h; f) Nano ExhibB- 1720 h. Inset in each figure corresponds to the topology profile of the deepest erosion channel, measured from HV electrode edge outwards, for each sample at time of record.

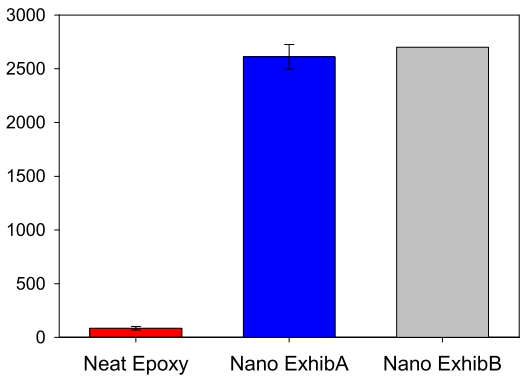


**FIGURE 6.** Voltage endurance lifetime for 1.6 mm thick samples voltage edurance tested under 12.5 kV/mm (312 VPM) in accordance with IEEE 1043/1553 standards. Nano ExhitB samples survied the test without a single failure.

thermal conductivities were set at 0.25 W/(m·K) for MIM and 0.7 W/(m·K) for NIM, respectively. Figure 7 shows the model containing 1/12$^{th}$ of the lateral cross-section of the machine.

### B. ELECTROMAGNETIC MODEL - ANSYS MAXWELL MODEL

The geometry from RMxprt was then imported to Maxwell and the machine structural parameters, electromagnetic

**TABLE 2.** Propulsion motor design parameters [21], [22].

| | | | |
|---|---|---|---|
| **Machine** | | | |
| Number of Poles | 24 | Reference Speed | 193 RPM |
| **Machine → Stator** | | | |
| Outer Diameter | 1170 mm | Inner Diameter | 950 mm |
| Length | 1000 mm | Number of Slots | 144 |
| **Machine → Stator → Slot** | | | |
| Hs0 | 1 mm | Hs1 | 2.5 mm |
| Hs2 | 75 mm | | |
| **Machine → Stator → Winding** | | | |
| Coil Pitch | 5 | Number of Strands | 1 |
| **Machine →Rotor** | | | |
| Number of Slots | 108 | Outer Diameter | 948 mm |
| Inner Diameter | 180 mm | Length | 1000 mm |
| **Machine → Rotor → Winding** | | | |
| Bar Conductor | Copper | End Length | 25 mm |
| End Ring Width | 25 mm | End Ring Height | 25 mm |
| **Analysis → Setup** | | | |
| Rated Output Power | 4500 HP | Rated Voltage | 4160 V |
| Rated Speed | 193 RPM | Operating Temperature | 75°C |
| Winding Connection | Wye | Frequency | 40 Hz |

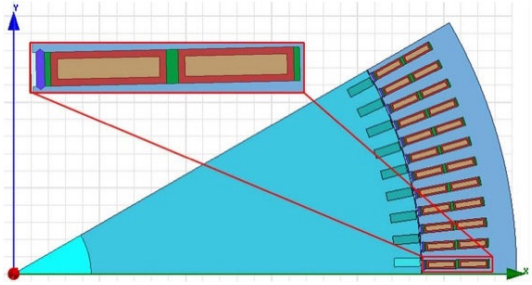

**FIGURE 7.** 2D Geometry of FEA model of the medium voltage induction machine with insulation layer.

parameters and operating conditions were set up in Maxwell, which generates automatically the corresponding machine geometry and excitation. The model was then used to evaluate the dependence of machine properties, i.e., torque characteristics and efficiency, on electromagnetic design and constitutive parameters. Figure 8 shows the similar total losses between the motors with NIM and with MIM at rated working conditions.

### C. THERMAL MODEL–ANSYS STEADY STATE

The thermal model was constructed using the ANSYS SteadyState Thermal analysis software by importing the geometry from the 2D FEA model. It also imports electrical losses as heat sources. Multiphysics coupling of EM and thermal modeling was conducted by linking ANSYS Maxwell and ANSYS SteadyState with ANSYS Workbench as shown in Figure 9. Figure 10 shows the imported heat sources. Figure 11 illustrates the thermal boundary conditions, including convective boundary between outer case of the stator and the air (A), radiative boundary at outer case of

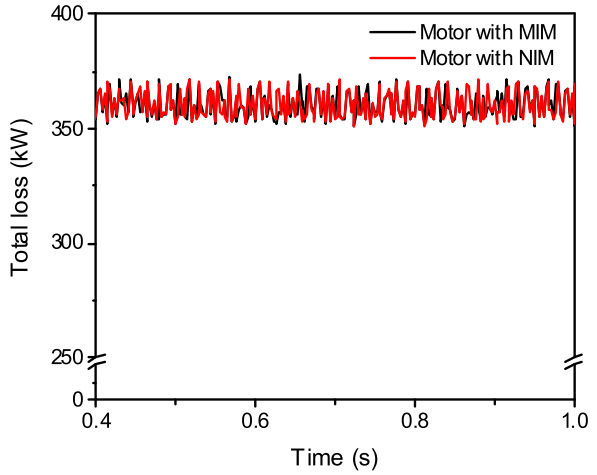


**FIGURE 8.** Comparison of machine total loss at steady state for motors with MIM and NIM.

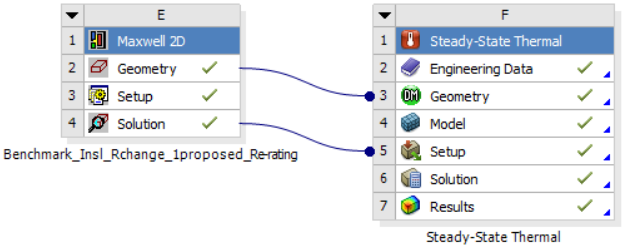


**FIGURE 9.** ANSYS Workbench linking the electromagnetic (ANSYS Maxwell) and thermal models (ANSYS SteadyState).

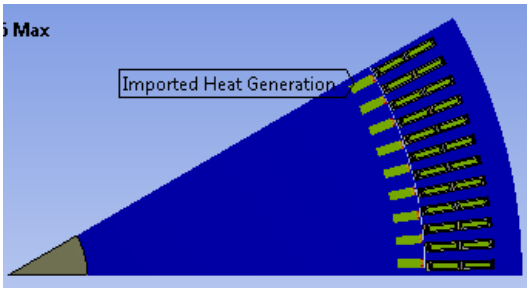


**FIGURE 10.** Imported heat sources in ANSYS Steady State.

the stator and the air (B), convective boundary between rotor core (steel – gray color in the zoomed-in picture of Figure 11) and the air gap between stator and rotor (C), convective boundary between the rotor copper bars (dark brown color in the zoomed-in picture of Figure 11) and the air gap between stator and rotor (D), convective boundary between the stator wedge (pink color in the zoomed-in picture of Figure 11) and air gap between stator and rotor (E), and outer boundary of the rotor shaft (F). The key heat transfer parameters for the thermal simulation are summarized in Table 3 .

The thermal model analysis was performed for 4 cases with different temperature boundary conditions, as shown in Table 4 . In cases 1 and 2, the temperature at A, B, and F is 18°C and 22°C, respectively, which corresponds to ambient room temperature. In cases 3 and 4, the temperature at A,

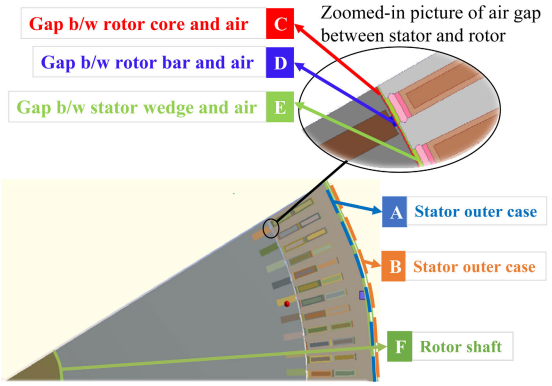


**FIGURE 11.** Thermal boundary conditions.

**TABLE 3.** Thermal boundary conditions and heat transfer parameters.

| Boundary | Description | Condition | Coefficient |
|---|---|---|---|
| A | Heat transfer - outer case of the stator | Convection | 1050 W/(m$^2$·K) |
| B | Heat transfer - outer case of the stator | Radiation | Emissivity - 0.85 |
| C | Heat transfer between the rotor core (steel) and the air gap between stator and rotor | Convection | 1050 W/(m$^2$·K) |
| D | Heat transfer between rotor copper bars and the air gap between stator and rotor | Convection | 1160 W/(m$^2$·K) |
| E | Heat transfer between the stator wedge (in pink color) and air gap between stator and rotor | Convection | 100 W/(m$^2$·K) |
| F | Heat transfer at rotor shaft outer boundary | Constant temperature | N/A |

**TABLE 4.** Maximum and minimum temperatures (°c) in motor with nanostructured insulation vs motor with mica.

| Case | Boundary Conditions at A, B, F (°C) | Temperature in the Motor with Proposed Material (NIM) | | Temperature in the Motor insulated with Mica (MIM) | |
|---|---|---|---|---|---|
| | | $T_{min}$ | $T_{max}$ | $T_{min}$ | $T_{max}$ |
| 1 | 18 | 18 | **105.1** | 18 | **144.04** |
| 2 | 22 | 22 | **109.06** | 22 | **148.04** |
| 3 | 40 | 40 | **127.05** | 40 | **166.04** |
| 4 | 58 | 58 | **145.05** | 58 | **184.04** |

B, and F is set at elevated ambient temperature of 40°C and 58°C, respectively, which demonstrates hot working environment of the motor. The maximum and minimum temperature inside the motor of the thermal simulation results is shown in Table 4 . An example of temperature profiles for case 4 is illustrated in Figure 12 for both MIM and NIM. As seen in Figure 12 and Table 4, the maximum temperature of the motor concentrates at the copper stator bar and increases correspondingly to the rise of temperature at A, B, and F. When the ambient temperature is 58°C (case 4), the maximum

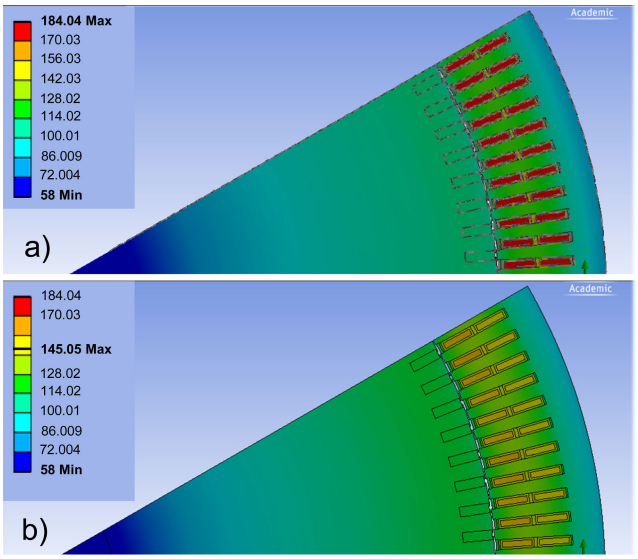


**FIGURE 12.** Temperature profiles of (a) MIM and (b) NIM for Case 4 in Table 4 .

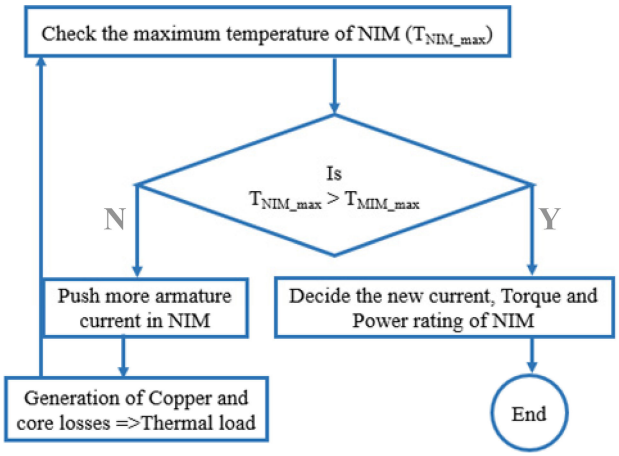


**FIGURE 13.** Rerating process of the NIM with respect to MIM to obtain $T_{MIM\_max}$.

temperature in motor with MIM reaches 184.04°C, while that of motor with NIM is only 145.05°C. In all 4 cases, the maximum temperature of motor with the proposed nanostructured insulation material NIM (thermal conductivity of 0.7 W/(m·K)) is constantly lower than that of motor with conventional micaceous insulation material MIM (thermal conductivity of 0.25 W/(m·K)) by about 40°C, depicting the critical role of insulation material thermal conductivity on the motor thermal performance.

### D. TORQUE DENSITY UPRATING

After obtaining results from Table 4 for all four cases, it is clear that motor with NIM has more room for current draw and thus torque production before it reaches the maximum temperatures of NIM. Therefore, NIM is iteratively re-rated as shown in Figure 13 to match the temperature profile of MIM by pushing in more torque. Iterations are performed until $T_{NIM\_max} = T_{MIM\_max}$.

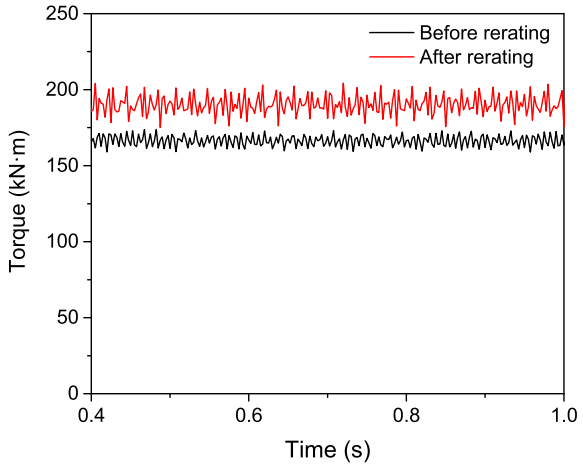


**FIGURE 14.** Torque of motor with NIM before and after rerating to match the maximum temperature of motor with MIM for Case 1 in Table 4.

The rerated torque of NIM in the case 1 of Table 4 is shown in Figure 14. The torque that can be achieved in the same machine when reaching the MIM maximum temperature of the same case is about 190 kN·m, which is 14% higher than that before rerating (166 kN·m). Studies based on other cases in Table 4, in addition to several cases not listed in this paper, all achieved similar torque enhancement. The studies clearly show the torque density uprating opportunity enabled by this novel nanostructured insulation material.

## IV. CONCLUSION

Nanostructured high-performance MV motor winding insulation based on epoxy with 2D platelet nanofillers has been successfully developed. Design of Experiment has been carried out to identify the optimal formulations with superior electrical discharge resistance and >2X combined improvement in electrical and heat transfer over the state-of-the-art micaceous insulation. Machine re-rating studies based on Multiphysics coupled EM and thermal modeling on representative propulsion motor design indicated a highly enhanced torque rating by 14% with this new 2D nano-structured insulation for all the boundary conditions studied, indicating a clear pathway to increase the payload efficiency of MV marine electric propulsion. This development holds the promising as the first major development in rotating machine insulation for over half a century with game changing characteristics. In addition, not only will this paradigm shift render in motor with higher payload efficiency and torque density, but also new eco-friendly and highly productive manufacturing processes. Furthermore, this technology will branch out into other critical components of IPS such as generators, trans- formers, circuit breakers, Electromagnetic Aircraft Launch System (EMALS), and, most importantly, broader industrial applications.

## ACKNOWLEDGMENT

The authors would like to thank Electric Boat, a General Dynamic Company, for in-kind support and technical guidance.

## REFERENCES


[1] *Naval Science and Technology Strategic Plan*, Office Naval Res., Arlington, VA, USA, 2011.

[2] *Naval Power and Energy Systems Technology Development Roadmap*, Naval Sea Syst. Command, Washington Navy Yard, DC, USA, 2019.

[3] *Surface Warfare Enterprise Science and Technology Strategic Plan*. Accessed: Dec. 24, 2020. [Online]. Available: https://www.onr.navy.mil/-/media/Files/Funding-Announcements/Special-Notice/2013/13-SN-0023-SWE-Plan.ashx

[4] *Naval Engineering in the 21st Century: The Science and Technology Foundation for Future Naval Fleets*. Washington, DC, USA: Academies, 2011.

[5] N. Doerry, "Next generation integrated power systems," in *NGIPS Master Plan*. Washington, DC, USA: Naval Sea Systems Command, 2007.

[6] B. A. Bassham, "An evaluation of electric motors for ship propulsion," M.S. thesis, Naval Postgraduate School, Monterey, CA, USA, 2003.

[7] C. Lewis, "The advanced induction motor," in *Proc. IEEE Power Eng. Soc. Summer Meeting*, Jul. 2002, pp. 250–253.

[8] J. S. Thongam, M. Tarbouchi, A. F. Okou, D. Bouchard, and R. Beguenane, "All-electric ships—A review of the present state of the art," in *Proc. 8th Int. Conf. Exhib. Ecol. Vehicles Renew. Energies (EVER)*, Mar. 2013, pp. 1–8.

[9] M. Frank, G. Nerowski, J. Frauenhofer, R. Hartig, W. Rzadki, P. van Hasselt, P. Kummeth, P. Massek, W. Nick, H. Rothfischer, H. Schmidt, B. Wacker, and H.-W. Neumuller, "High-temperature superconducting rotating machines for ship applications," *IEEE Trans. Appl. Supercond.*, vol. 16, no. 2, pp. 1465–1468, Jun. 2006.

[10] H. E. Lundquist, "DDG 1000's integrated power system software, hardware come together in successful test," defensemedianetwork.com, St. Petersburg, FL, USA, Tech. Rep. Accessed: Dec. 24, 2020. [Online]. Available: https://www.defensemedianetwork.com/stories/ddg-1000s-integrated-power-system-software-hardware-come-together-in-successful-test/

[11] Leonardo DRS, Arlington, VA, USA. *Integrated Marine Systems*. Accessed: Dec. 24, 2020. [Online]. Available: https://www.leonardodrs.com/media/8803/leonardo-drs-marine-systems-catalog.pdf

[12] *Permanent Magnets Motor and Generators*, Gamesa Electric, 2014.

[13] M. K.-F. Lee and Y. Cao, "Apparatus for forming insulation for electrical components," U.S. Patent 9 293 972, Mar. 22, 2016.

[14] D. Schneider, "Clad in controversy," *IEEE Spectr.*, vol. 50, no. 8, pp. 32–37, Aug. 2013.

[15] G. C. Stone and G. H. Miller, "Progress in rotating-machine insulation systems and processing," *IEEE Elect. Insul. Mag.*, vol. 29, no. 4, pp. 45–51, Jul./Aug. 2013.

[16] G. Stone, E. A. Boutler, I. Gilbert, and H. Dhirani, *Electrical Insulation for Rotating Ma-chines*. Hoboken, NJ, USA: Wiley, 2004.

[17] J. Wadsworth, G. W. Crabtree, R. J. Hemley, R. Falcone, I. Robertson, J. Stringer, P. Tortorelli, G. T. Gray, M. Nicol, J. Lehr, S. W. Tozer, T. D. de la Rubia, T. Fitzsimmons, J. S. Vetrano, C. L. Ashton, S. Kitts, C. Landson, B. Campbell, G. Gruzalski, and D. Stevens, "Basic research needs for materials under extreme environments," in *Proc. Rep. Basic Energy Sci. Workshop Mater. Under Extreme Environ.* Washington, DC, USA: US DOE—Office of Basic Energy Sciences, Jun. 2007, doi: 10.2172/935440.

[18] G. Griffith, S. Tucker, J. Milsom, and G. Stone, "Problems with modern air-cooled generator stator winding insulation," *IEEE Elect. Insul. Mag.*, vol. 16, no. 6, pp. 6–10, Nov. 2000.

[19] Y. Cao, P. C. Irwin, and K. Younsi, "The future of nanodielectrics in the electrical power industry," *IEEE Trans. Dielectr. Electr. Insul.*, vol. 11, no. 5, pp. 797–807, Oct. 2004.

[20] H. Nguyen, Y. Liu, W. Chen, M. Ghassemi, J. Chapman, A. Bazzi, and Y. Cao, "Nanostructured insulation for high torque density electric propulsion motors," in *Proc. IEEE Electr. Ship Technol. Symp. (ESTS)*, Arlington, VA, USA, Aug. 2017, pp. 274–279.

[21] Y. Liu, H. Nguyen, A. M. Bazzi, and Y. Cao, "Torque enhancement and re-rating of medium-voltage induction machines using nano-structured stator winding insulation," in *Proc. IEEE Electr. Ship Technol. Symp. (ESTS)*, Arlington, VA, USA, Aug. 2017, pp. 232–237.

[22] D. Cook, "Integrated systems approach to induction motor selection and design," in *Proc. Elect. Mach. Tech. Symp.* Richmond, VI, USA: American Society of Naval Engineers, 2014.


**HIEP HOANG NGUYEN** (Member, IEEE) received the B.S. and M.S. degrees (Hons.) in electrical engineering from Tomsk Polytechnic University, Russia, in 2009 and 2011, respectively. He is currently pursuing the Ph.D. degree with the University of Connecticut, USA. His research interests include development of new nanostructured dielectrics, high voltage testing and characterization of electrical insulation material, and power systems.

**ARSHIAH Y. MIRZA** (Graduate Student Member, IEEE) received the B.Tech. degree in electrical and electronics engineering from SNIST affiliated to Jawaharlal Nehru Technological University, Hyderabad, India, in 2016, and the M.S. degree in electrical and computer engineering from the University of Connecticut, USA, in 2019, where she is currently pursuing the Ph.D. degree. Her research interests include power electronics, machine drives, and high voltage insulation testing.

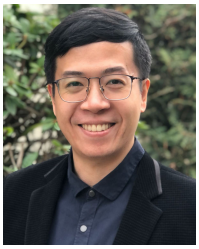

**WEIQIANG CHEN** (Member, IEEE) received the M.S. and Ph.D. degrees in electrical and computer engineering (ECE) from the University of Connecticut (UCONN), Storrs, CT, USA, in 2014 and 2019, respectively. He was a Student Intern at Bosch Automotive Diesel System Company, Ltd., Wuxi, China, from February to June 2012, and an Electrical Intern at IMCOPR from August 2018 to March 2019. He joined IMCORP as a Senior Power Electronics Design Engineer in 2019. His research interest mainly focuses on fault diagnosis and optimization of power electronic systems, high power converters, wireless charging topologies, and machine drives.

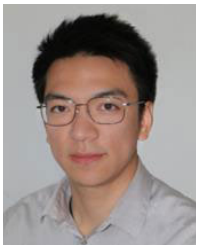

**YIQI LIU** received the M.S. and Ph.D. degrees in electrical engineering from the University of Connecticut, Storrs, CT, USA, in 2016 and 2017, respectively. He was an Intern at UTC Climate, Controls & Security, in Summer 2016, and at Tesla, in Fall 2017. He joined John Deere Electronic Solutions, in 2018, as a Power Electronics Control Software Engineer. His research interests include modeling, control, analysis, and optimization of electric motor drive systems, and power electronics for machine electrification applications.

**JOANNE RONZELLO** was graduated in chemistry and electrical engineering. She is currently a Research Assistant with the Electrical Insulation Research Center, Institute of Materials Science, University of Connecticut. She has spent more than 36 years working in the area of dielectrics including, high voltage testing, failure analysis, dielectric spectroscopy, and novel experimental development.

**JACK CHAPMAN,** photograph and biography not available at the time of publication.

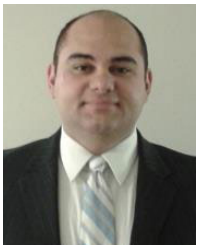

**ALI M. BAZZI** (Senior Member, IEEE) received the B.E. and M.E. degrees in electrical engineering from the American University of Beirut, Beirut, Lebanon, in 2006 and 2007, respectively, and the Ph.D. degree from the University of Illinois at Urbana-Champaign (UIUC), Urbana, IL, USA, in 2010. He joined the University of Connecticut (UCONN), USA, in 2012, as an Assistant Professor, where he established and currently directs the Power Electronics & Drives Advanced Research Laboratory (PEARL). He was a Senior Power Electronics Electrical Engineer with Delphi Electronics and Safety, from 2011 to 2012, a Visiting Assistant Professor with UIUC, in Spring 2011, an Engineer with Bitrode Corporation, in the summers of 2008 and 2009, and a Research and Teaching Assistant with UIUC, from 2007 to 2010. In 2016, he became an UTC Assistant Professor of Engineering Innovation at UCONN, where he is currently an Associate Professor of Electrical and Computer Engineering (ECE). His research interests include power electronics design, control, optimization, fault diagnosis, and reliability modeling in motor drives, solar photovoltaics, and other applications. He is also interested in renewable energy integration in micro-grids, and real-time control and optimization of energy systems in general. He has served on the organizing and technical committees of many IEEE conferences. He received the NSF CAREER Award in 2018, the Mavis Memorial Scholarship from UIUC, in 2009, the Outstanding Teaching Award from the ECE Department, UCONN, in 2014, and the Research Excellence Award from UCONN, in 2015 and 2018. He has more than 90 peer-reviewed and refereed technical publications and holds several patents. He is a member of the IEEE Industry Applications Society, the IEEE Power Electronics Society, the IEEE Power and Energy Society, and the IEEE Industrial Electronics Society.

**YANG CAO** (Senior Member, IEEE) received the B.S. and M.S. degrees in physics from Tongji University, Shanghai, China, and the Ph.D. degree from the University of Connecticut, in 2002. From 2002 to 2013, he served as a Senior Electrical Engineer with the GE Global Research Center. He is currently a Full Professor with the Electrical and Computer Engineering Department, University of Connecticut. He is also the Director of the Electrical Insulation Research Center, Institute of Materials Science, and the Site Director of the NSF I/UCRC Center on High Voltage/Temperature Materials & Structures. His research interests include the physics of materials under extremely high field and the development of new dielectric materials, particularly the polymeric nanostructured materials, for energy efficient power conversion and renewables integrations, as well as for novel medical diagnostic imaging devices. He is active in both the Dielectric and Electrical Insulation Society and Power and Energy Society. He is an Associate Editor of the IEEE TRANSACTIONS ON DIELECTRICS AND ELECTRICAL INSULATION.